ISSN 1027-4510, Journal of Surface Investigation. X-ray, Synchrotron and Neutron Techniques, 2008, Vol. 2, No. 2, pp. 310–316. © Pleiades Publishing, Ltd., 2008.
Original Russian Text © I.I. Tashlykova-Bushkevich, E.S. Gut'ko, V.G. Shepelevich, S.M. Baraishuk, 2008, published in Poverkhnost'. Rentgenovskie, Sinkhrotronnye i Neitronnye Issledovaniya, No. 4, pp. 69–75.

Structural and Phase Analysis of Rapidly Solidified Al–Fe Alloys

I. I. Tashlykova-Bushkevich[a], E. S. Gut'ko[b], V. G. Shepelevich[b], and S. M. Baraishuk[c]

[a] *Belarusian State University of Informatics and Radioelectronics, ul. P. Brovki 6, Minsk, 220013 Belarus*
[b] *Belarusian State University, ul. F. Skoryny 4, Minsk, 220080 Belarus*
[c] *Belarussian State Pedagogical University, Sovetskaya ul. 18, Minsk, 220050 Belarus*

Received September 20, 2007

Abstract—The structure and phase composition of lightly-doped Al–Fe alloys obtained by ultrarapid quenching from the melt are investigated. The surface of foils was studied using scanning electron microscopy, atomic-force microscopy, and Rutherford backscattering technique. The variation in the phase composition of alloys during annealing was studied by x-ray diffraction technique and by resistivity and microhardness measurements. The Al–Fe alloys have microcrystalline structure with a nonuniform iron content in the near-surface region of the samples. A correlation of depth profiles of iron and phase composition of the foils is observed. It is found that decomposition of the supersaturated α solid solution proceeds in the temperature range 250–350°C. As the annealing temperature increases, a metastable Al_6Fe phase is precipitated. In the range 300–500°C, the metastable Al_6Fe phase decomposes, and a stable Al_3Fe phase is precipitated.

DOI: 10.1134/S1027451008020286

INTRODUCTION

It is known that ultrarapid quenching from the melt (USQM) of aluminum alloys leads to the formation of materials with a unique microstructure due to varying the chemical composition, formation of metastable phases, and varying the structure [1, 2]. The purpose of this study was to analyze the structure of the rapidly solidified (RS) foils of lightly-doped Al–Fe alloys depending on the treatment temperature and phase composition of the samples. The use of the USQM method is considered promising for increasing such working characteristics of alloys of the Al–Fe system as strength and plasticity [3]. There are numerous works devoted to the structure and properties of RS Al–Fe alloys. Despite this fact, their study remains topical due to interest caused by their possible use as high-temperature alloys in the aerospace industry [4–7]. The iron distribution in RS samples including the variation in the layer-by-layer elemental composition of the Al–Fe alloys during the phase transformations is insufficiently investigated.

The surface of RS foils of the Al–Fe alloys was studied using scanning electron microscopy and atomic-force microscopy. Investigation of spatial distribution of iron in foils of aluminum alloys was also continued [8, 9] using Rutherford backscattering (RBS) technique and the computer simulating programs RUMP [10, 11]. To determine the stability of alloys, x-ray structural analysis of the foils was performed in combination with the measurements of resistivity and microhardness after annealing. Preference of the measurement of electrical conductivity during investigation of phase transformations in the RS Al–Fe alloys was reported in [12]. In this work, interrelation of layer-by-layer elemental and phase composition of the Al–Fe alloys is also discussed.

EXPERIMENTAL

To fabricate the samples, we used aluminum of 99.99% grade. The alloys Al–0.25, 0.3, 0.5, 0.6, 1.0, and 1.5 at % Fe were obtained by alloying the mixture of components in an ISV-0.004-PI-M1 induction vacuum electrical furnace. RS foils of 50–70 μm in thickness and width 5–10 mm were obtained by slopping the melt drop on the inner surface of rotating copper cylinder by the method described in detail in [13]. The cooling rate of the melt was ~10^6 K/s [14]. Surface topography of the samples was studied using a JEOL1455VP scanning electron microscope. Three-dimensional (3D) images of the surface of the foils under study were obtained using an NT-206 atomic-force microscope (AFM). Iron distribution over the alloy depth was investigated at the Friedrich Schiller University of Jena, Germany, by the method of Rutherford backscattering (RBS) of helium ions with an energy of 1.4 MeV and energy resolution of 17 keV with the following experimental geometry: $\theta_1 = 0°$, $\theta_2 = 10°$, $\theta = 170°$, where θ_1, θ_2, and θ are the angles of flight in, flight out, and scattering of ions, respectively. The experimental spectra of backscattering were processed with the use of the computer modeling programs RUMP, which allows one to investigate the concentrations of elements in the sam-

ples starting from 0.001 at %. The yield of pulses Y in the spectra is a set of random digits depending on the number of scattered particles entered the detector. Since in this case we do not speak about the systematic error, the relative error in determining the iron concentration was calculated as the statistical error and did not exceed 6%: $\varepsilon_{Fe} = (Y_{Fe})^{1/2}/Y_{Fe}$ [15, 16], where Y_{Fe} is the number of signal pulses from iron. X-ray diffraction analysis of the phase composition of alloys and determination of the unit cell parameter of the foils depending on the annealing temperature of the samples was carried out using a DRON-3M diffractometer (copper radiation). To calculate the lattice parameter a of the foils, we studied the (400) diffraction line from aluminum; the error in determining a was no larger than 0.02% [17]. Microhardness H_μ of alloys was measured using a PMT-3 device under the load of 20 g accurate to 5%. Isothermal annealing was carried out at constant temperatures for one hour at each temperature. Isochronous annealing of the samples was performed sequentially through 30–40°C holding for 20 min at each temperature. To determine the ratio of resistivities $\rho(T)/\rho_0$, we used the probe method with the relative error in determination of $\rho(T)/\rho_0$ down to 1%.

RESULTS AND DISCUSSION

Investigation of morphology of RS Al–Fe alloys shows that on the surface contacting with the substrate (cylinder) cavities are formed, in which a cellular structure consisting of elongated or two-dimensional cells and isolated grooves is observed (Fig. 1a). Additionally, certain cells and grooves associated with the grain boundaries are graphically marked. The surface of foils contacting with air has a cellular structure (Fig. 1b). The size of the cells of the foils of the Al–0.6Fe alloy is from 0.5 to 2.0 μm. On the sample surface, roughness is observed on both sides, and the relief of foils on the side contacting with the substrate is smoother than on the outer side. Figure 1d shows a three-dimensional image of the surface of the Al–0.3Fe alloy contacting with the substrate.

We measured the iron distribution in the near-surface region of the foils of the Al–0.3Fe alloy contacting in the surface. In a thin (~0.3 μm) near-surface layer of the foils, an increased iron content reaching 1.35 at % is observed. In the near-surface region (from 0.1 to 0.7 μm), iron is distributed virtually uniformly (Fig. 2). The average iron concentration is 0.33 at %.

Investigation of microhardness of the foils of the Al–Fe alloys during isochronous and isothermal annealing indicates that annealing of alloys at relatively low temperatures (up to 110°C) causes a small increase in H_μ (Figs. 3a, 3b). An increase in the temperature of isochronous annealing leads to a virtually monotonic decrease in microhardness of foils of the Al–0.6 and 1.0 Fe alloys (Fig. 3a). The qualitatively comparable behavior of the microhardness is also observed during isothermal annealing of Al–0.6Fe alloy foils (Fig. 3b). In the same range of annealing temperatures, a decrease in resistivity $\rho(T)/\rho_0$ is observed (Fig. 3c).

Upon heating the foils to 100°C, the unit cell parameter a of the foils of the Al–0.5Fe alloy remains invariable and equal to 0.4047 nm. The further isochronous annealing in the temperature range from 100 to 250°C leads to a decrease in the values of the unit cell parameter (Fig. 4). For example, after annealing the samples at 200°C, a = 0.4044 nm. After annealing at above 200°C, an increase in the unit cell parameter is observed. The unit cell parameter of pure aluminum equals 0.4049 nm [18].

Analysis of x-ray diffraction patterns of the foils of the Al–1.5Fe alloy indicates that annealing at 230°C for 2 h leads to decomposition of the supersaturated aluminum-based solid solution and precipitation of a metastable Al_6Fe phase. We obtained the coincidence of interplanar spacings of a new phase d_0 determined by the location of additional diffraction lines absent in the X-ray diffraction patterns of as-received foils and the values of interplanar spacings d_m calculated for the metastable Al_6Fe phase having an orthorhombic crystal lattice with the unit cell parameters a = 0.6492 nm, b = 0.7437 nm, and c = 0.7885 nm [19] (Table 1). We found no inclusions of the second phase in as-received RS alloys in the region of formation of a metastable supersaturated α-Al solid solution (iron concentration in the alloy up to 1.5 at %) [20].

Annealing of the foils of the Al–1.5Fe alloys in the temperature range 300–600°C initially leads to a decrease in intensity of diffraction lines of the metastable Al_6Fe phase and then to their disappearance. Simultaneously, we observed new diffraction lines belonging to a stable Al_3Fe phase having a monoclinic crystal lattice with the parameters a = 1.5520 nm, b = 0.8099 nm, c = 1.2501 nm, and α = 107°43' [19]. Table 2 presents interplanar spacings d_m calculated for the metastable Al_6Fe phase and interplanar spacings of a new phase d experimentally calculated for foils annealed at 500°C for 1 h. Since the values of d and d_m coincide, we can assume that a stable Al_3Fe phase is precipitated during decomposition of the aluminum-based solid solution at 500°C.

We previously found that the RS foils of lightly-doped Al–Fe alloys have a microcrystalline structure [21]. The average size of foil grains is several microns and decreases as the iron concentration in the alloy increases. The results of this investigation of the structure of the surfaces of the RS Al–Fe alloys shows that during URQM of the Al–Fe alloys, a cellular structure is formed similar to the structures found in the RS Al–Zn and Al–V alloys [13, 22, 23]. AFM studies indicate the presence of transverse inhomogeneity of the surface of foils along the Z axis, which constitutes on average ~0.01 μm. By the data [24], longitudinal sizes and distribution of air cavities on the surface of the foils of the Al–Cu alloys obtained by the method of melt spinning close to the URQM method used in this work depend on the drum material and its linear velocity.

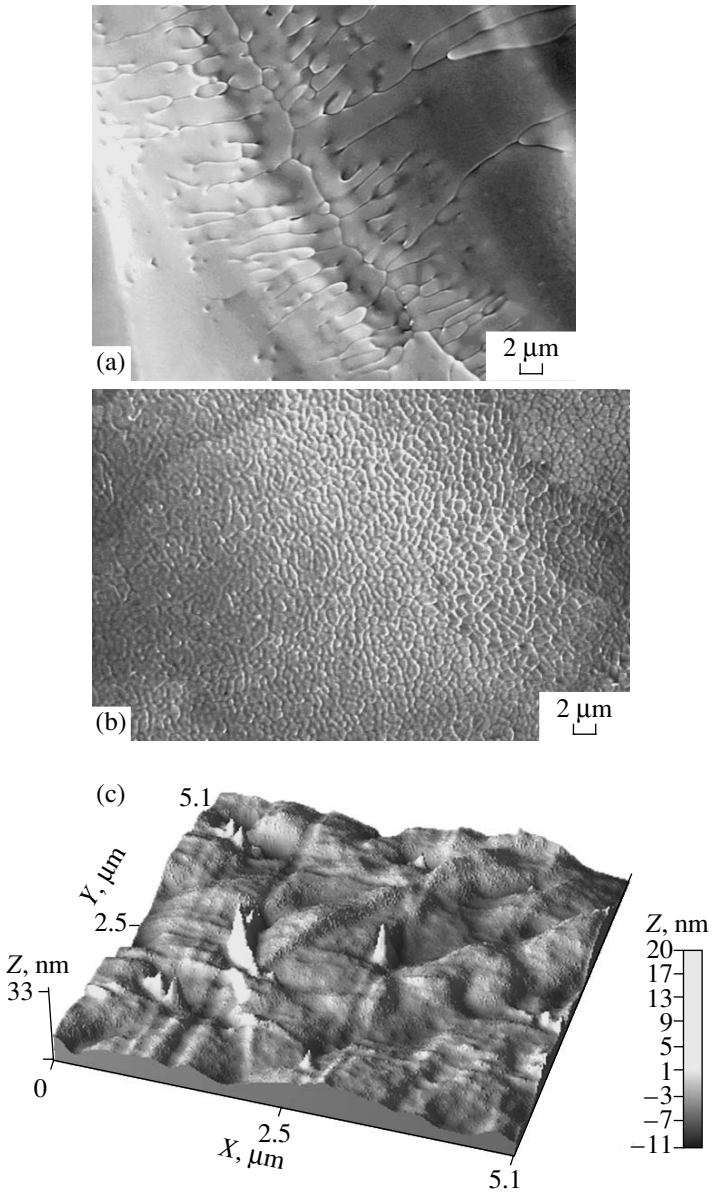

Fig. 1. Microstructure of the surface of the foils of the Al–0.6 Fe alloys contacting (a) with the substrate and (b) with air. (c) Typical 3D image of the surface of the Al–0.3 Fe alloy contacting with the substrate. (a) Certain cells and grooves related with grain boundaries are marked graphically.

Comparison of distribution profiles of iron over the depth of foils of the Al–0.3 Fe and Al–0.25, 2.0 Fe alloys obtained in the induction furnace and in quartz cells [8] allows us to formulate regularities of redistribution of the doping component of iron during the ultrarapid solidification of lightly-doped binary aluminum alloys. In a thin near-surface layer of all investigated objects, the iron content exceeds the eutectic concentration ~0.8 at % [25] by a factor of 1.7–2.5 and is above the experimentally measured concentration in the bulk by a factor of 4.5–6.9. Notice that an increase in the iron content in a thin near-surface layer of RS Al–Fe alloys corresponds to the data obtained for binary aluminum alloys containing Cu, Co, Ni, Ge, and Sb [26–30]. It is found that this effect is independent of the concentration of the doping element. It is known that the USQM process leads to an increase in the concentration of nonequilibrium vacancies in the alloy [31]. Vacancies are able to form mobile complexes "atom of dissolved element–vacancy" and diffuse to the surface, which is their sink, along with the doping element even at such high rates of cooling and solidification of the melt as during USQM [32–34]. Therefore, apparently, excess of the doping element is formed in a thin near-surface layer precisely due to the fact that the atoms of dissolved elements are transferred with vacancies in the direction of the surface of the foils and grain boundaries [33]. Based on the data on the grain structure of the RS

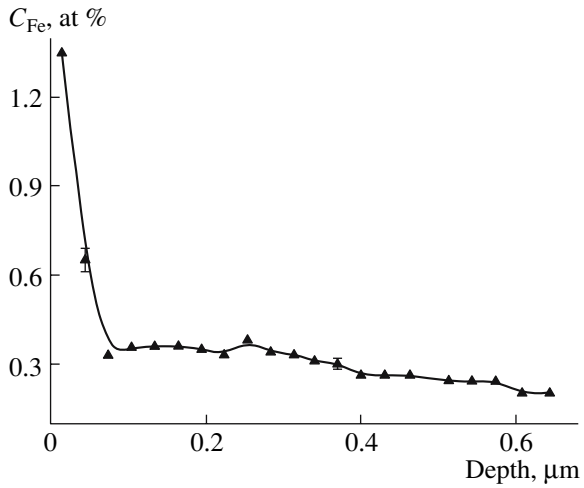

Fig. 2. Typical distribution profile of iron in the Al–0.3 Fe alloy over the depth obtained by modeling the RBS spectra from the surface of the samples contacting with the substrate using the RUMP program.

foils of the aluminum alloys [21], the layer-by-layer elemental analysis of RS alloys by the RBS method was performed over the depth of the columnar grain. The distribution of components in the grain is averaged over the section area of a beam 1 mm in diameter, which constitutes up to 10^5 columnar grains according to estimates. Comparison with the previously obtained RBS results for the Al–Fe alloys [8] confirms reproducibility of the data.

Therefore, we can conclude that interpretation of the results of the layer-by-layer elemental analysis carried out by the RBS method for the foils of aluminum alloys is realistic. The question of the effect of the surface roughness of the sample on the shape of the RBS spectra is considered in [35, 36]. It is stated that, first, in the case of beam incidence along the normal to the surface (the geometry considered in this work), the effect of roughness on the shape of the RBS spectrum is minimal. Second, for samples with a nonuniform surface, due to the presence of hills and valleys, the yield of particles in the high-energy region decreases. Due to this, the atomic concentration in the surface layer of the sample is below the actual value. However, this effect is insignificant if the beam size is comparable with the size of inhomogeneities [36]. In cast bulk samples, a nonuniform over the depth distribution of doping elements in the near-surface layer is not observed by the RBS method in the limits of depth resolution [37].

The authors of [6, 38] found that in the supersaturated Al–Fe solid solutions obtained by USQM, iron atoms are not statistically distributed in the aluminum lattice. It was reported [39] that the melts of the Fe–Al system are inhomogeneous and contain clusters. The bulk content of clusters depends on the concentration of alloy components. Therefore, a certain increase in microhardness at the initial stage of isochronous annealing and isothermal annealing at 60°C can be apparently associated with redistribution of iron atoms in the α solid solution, which leads to the additional formation of cluster groups enriched by iron atoms and

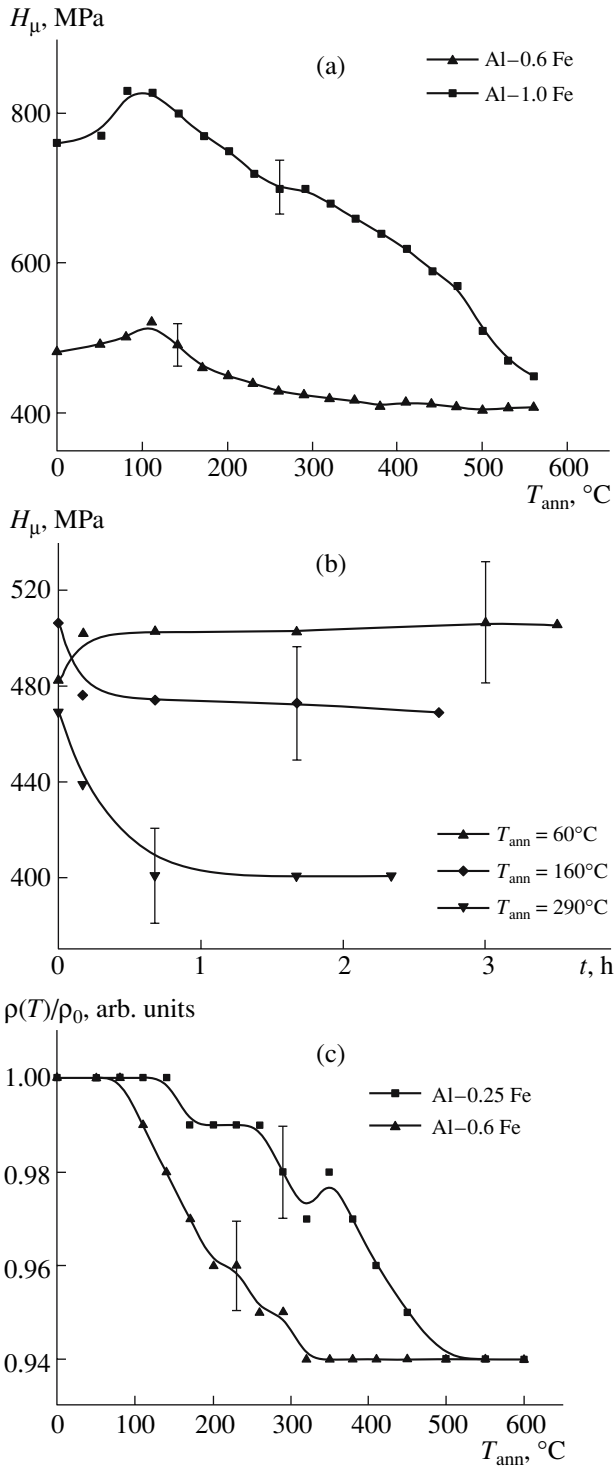

Fig. 3. Variation in microhardness $H_μ$ of the foils (a) of the Al–0.6 and 1.0 Fe alloys after isochronous annealing and (b) of the Al–0.6 Fe alloy after isothermal annealing. (c) Temperature dependence of the ratio ρ(T)/ρ$_0$ for the foils of alloys Al–0.25 and 0.6 Fe.

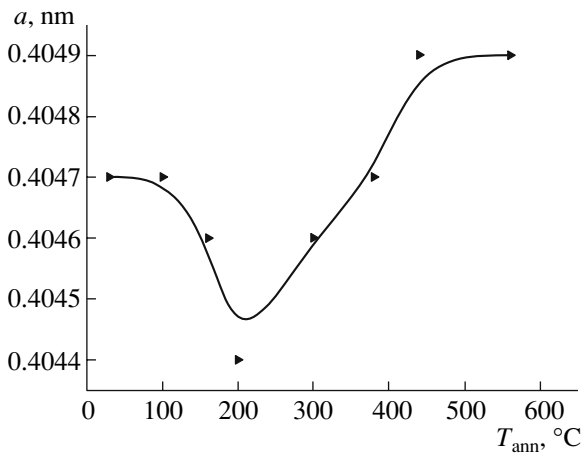

Fig. 4. Variation in the unit cell parameter a of the foils of the Al–0.5 Fe alloy after isochronous annealing.

is capable of causing strengthening of the alloys. In [40, 41], it was found that the formation of clusters leads to an increase in H_μ at the initial stage of annealing for the systems Al–Zn and Al–Mg with a high content of zinc and magnesium. The authors of [42] assumed that the decomposition of the supersaturated solid solution in the Al–Ge system starts from the formation of the Gunier–Preston zones strengthening the alloy. Further annealing in the temperature range 100–200°C leads to a decrease in the unit cell parameter of the alloy foils, which is associated with the decomposition of the Gunier–Preston zones. Partial destruction of cluster groupings and an increase in the fraction of iron atoms statistically distributed in the lattice was observed after annealing at 200°C of the RS Al–Fe alloys. This phenomenon, similarly to dissolution of the Gunier–Preston zones at the stage of preprecipitation, leads to a decrease in the parameter a [43]. Decomposition of the supersaturated aluminum-based solid solution, which is accompanied by depletion of a primary solid solution by iron atoms, causes a decrease in microhardness and resistivity of alloys. The decrease in resistivity after annealing points to precipitation of the atoms of the doping element and coagulation of inclusions [44–46]. The increase in the unit cell parameter of the foils of the Al–0.5 at % Fe alloy after annealing above 200°C also indicates the decomposition of the aluminum-based supersaturated solid solution. It follows from the curves of isochronous annealing that the process of precipitation and coagulation of iron-containing phases is dominant at the annealing temperature up to 500°C. The established temperature ranges of decomposition agree with the results [4, 47], where the Al alloys containing from 5.0 to 20.0 at % Fe obtained by melt spinning were studied.

Table 1. Comparison of interplanar spacings d_0 and d_m of the Al_6Fe phase

θ, deg	d_0, 10^{-4} μm	d_m, 10^{-4} μm	*hkl*
12.2	3.64	3.64	102
13.0	3.42	3.43	021
21.1	2.14	2.14	222
21.7	2.08	2.08	310
24.9	1.83	1.83	310

Table 2. Comparison of interplanar spacings d and d_m of the Al_3Fe phase

θ, deg	d, 10^{-4} μm	d_m, 10^{-4} μm	*hkl*
6.0	7.37	7.376	200
6.65	6.65	6.68	011
7.7	5.75	5.77	111
9.3	4.77	4.78	012
10.4	4.27	4.26	112
11.2	3.97	3.96	003
11.5	3.86	3.83	021
12.6	3.53	3.54	220
15.1	2.96	2.97	004
18.6	2.41	2.41	210
20.9	2.16	2.17	224
23.8	1.91	1.91	333
26.2	1.74	1.75	306
29.8	1.58	1.59	036
31.9	1.46	1.47	336
37.4	1.27	1.28	063

The fact that annealing at relatively low temperatures leads to the formation of clusters of iron atoms in the α solid solution can be explained by redistribution of elements in the foils of the Al–Fe alloys annealed at 140°C. We previously found the tendency to a decrease in the iron concentration in a thin near-surface layer at this temperature in alloys containing 0.25 and 2.0 at % Fe [8]. As the annealing temperature of the Al–2.0 Fe alloy increased to 500°C [8], a decrease in the iron concentration was observed on the surface of foils with a simultaneous increase of its content over the depth. It seems likely that the decrease in the concentration of the doping element is caused by its diffusion into the sample bulk. The probable cause of iron redistribution at 500°C is the decomposition of the metastable Al_6Fe phase and precipitation of the stable Al_3Fe phase. The effect of redistribution of elements due to annealing of the RS Al–Zn and Al–Ge alloys and the tendencies in the variation of the layer-by-layer composition of the foils with increasing the annealing temperature to 500°C was reported in [22, 23, 48]. Note that for the annealing of the RS Al–4.0 Zn and Al–5.0 Ge alloys, it is found that the concentration of the doping element in the thin near-surface layer increases as the annealing temperature increases. Thus, diffusion in the Al–Zn, Ge, and Al–Fe alloys during annealing proceeds in opposite directions: to the foil surface and to its depth. The character of zinc distribution over the depth in unannealed foils of the Al–Zn alloys—depletion of the

thin near-surface layer and an abrupt increase in the zinc content by a factor of 1.7–2.6 in the layer up to 0.2 μm and the subsequent virtually uniform zinc distribution over the sample depth—qualitatively differs from regularities of distribution of iron and germanium in the foils of the Al–Fe and Al–Ge alloys. To establish general regularities of distribution of elements over the depth of the foils of the Al alloys and to investigate the correlation of distribution profiles of doping elements and phase composition of alloys, it is necessary to continue the investigation of physical processes during USQM of aluminum alloys and during annealing of obtained foils.

CONCLUSIONS

Structural and phase analysis of the foils of the lightly-doped Al–Fe alloys is performed. During ultrarapid quenching, a cellular structure is formed on the surface of the foils contacting with air; the cell size varies from 0.5 to 2.0 μm. Cavities are formed on the surface contacting with a substrate; in these cavities, the cellular structure is also observed. For the first time, a transverse nonuniformity of the surface of the foils of the Al–Fe alloys equal to ~0.01 μm is established. A thin near-surface layer is enriched by iron: for the Al–0.3 Fe alloy, the iron concentration exceeds the calculated value by a factor of 4.5. Annealing of the Al–Fe alloys at the initial stage at the temperature ~110°C leads to an insignificant increase in microhardness, which can be explained by redistribution of iron atoms in the α solid solution, which leads to the formation of their clusters. During the subsequent increase in the annealing temperature of the foils, decomposition of the supersaturated aluminum-based solid solution takes place. The decomposition is accompanied initially by precipitation of the metastable Al_6Fe phase with the subsequent precipitation of the stable Al_3Fe phase.

ACKNOWLEDGMENTS

We thank Prof. W. Wesch, Friedrich Schiller University of Jena, Germany, for help in carrying out the experiments with the use of the RBS method.

REFERENCES

1. L. Katgerman and F. Dom, Mater. Sci. Eng., A **375–377**, 1212 (2004).
2. E. J. Lavernia, J. D. Ayers, and T. S. Srivatson, Int. Mater. Rev. **37** (1), 1 (1992).
3. R. F. Cochrane, P. V. Evans, and A. L. Greer, Mater. Sci. Eng., A **133**, 803 (1991).
4. D. H. Kim and B. Cantor, J. Mater. Sci. **29**, 2884 (1994).
5. T. I. Anishchenko, B. N. Litvin, and L. M. Burov, *Structure and Properties of Al–Fe Alloys Produced under Nonequilibrium Conditions* (Dnepropetrovsk University, Dnepropetrovsk, 1990) [in Russian].
6. I. G. Brodova, V. O. Esin, I. V. Polents, et al., Rasplavy, No. 1, 16 (1990).
7. M. Bizjak and L. Kosec, Z. Metallkd. **91** (2), 160 (2000).
8. I. I. Tashlykova-Bushkevich and V. G. Shepelevich, Fiz. Khim. Obrab. Mater., No. 6, 73 (1999).
9. I. I. Tashlykova-Bushkevich, Vacuum **78** (2–4), 529 (2005).
10. F. F. Komarov, M. A. Kumakhov, and I. S. Tashlykov, *Non-Destructive Ion Beam Analysis of Surfaces* (Universitetskoe, Minsk, 1987; Gordon and Breach, New York, 1990).
11. L. N. Doolittle, Nucl. Instrum. Methods Phys. Res., Sect. B **9**, 344 (1985).
12. M. Bizjak, L. Kosec, B. Kosec, and I. Anzel, Metalurgija (Zagreb, Croatia) **45** (4), 281 (2006).
13. I. I. Tashlykova-Bushkevich, V. G. Shepelevich, and E. Yu. Neumerzhitskaya, Poverkhnost, No. 4, 69 (2007).
14. S. I. Miroshnichenko, *Quenching from the Liquid State* (Metallurgiya, Moscow, 1982) [in Russian].
15. I. I. Tashlykova-Bushkevich, *Method of Rutherford Backscattering for Analysis of Compositions of Solids* (Belarussian State University of Informatics and Radioelectronics, Minsk, 2003) [in Russian].
16. G. L. Squires, *Practical Physics* (Wiley, London, 1968; Mir, Moscow, 1971).
17. A. A. Rusakov, *X-ray Diffraction of Metals* (Atomizdat, Moscow, 1977) [in Russian].
18. *Aluminum: Properties and Physical Metallurgy (Reference Book)*, Ed. by J. E. Hatch (The American Society for Metals, Metals Park, Ohio (United States), 1984; Metallurgiya, Moscow, 1989).
19. M. Hansen and K. Anderko, *Constitution of Binary Alloys* (McGraw-Hill, New York, 1958; Metallurgizdat, Moscow, 1962), Vol. 2.
20. E. Yu. Vasilevich, E. S. Gut'ko, and V. G. Shepelevich, *Theoretical and Technological Foundations of Hardening and Restoration of Products of Mechanical Engineering: Collected of Papers* (Polotsk State University, Polotsk, 2001), p. 162 [in Russian].
21. V. G. Shepelevich, I. I. Tashlykova-Bushkevich, and A. G. Anisovich, Fiz. Khim. Obrab. Mater., No. 4, 86 (1999).
22. I. I. Tashlykova-Bushkevich, E. S. Gut'ko, and V. G. Shepelevich, Perspekt. Mater., No. 1, 59 (2005).
23. I. I. Tashlykova-Bushkevich, E. S. Gut'ko, and V. G. Shepelevich, Adv. Mater. **12** (1), 54 (2005).
24. M. A. Taha, N. A. El-Mahallawy, and M. F. Abedel-Ghaffar, J. Mater. Sci. **27**, 5823 (1992).
25. A. P. Gulyaev, *Physical Metallurgy* (Metallurgiya, Moscow, 1986; Mir, Moscow, 1980).
26. I. I. Tashlykova-Bushkevich and V. G. Shepelevich, J. Alloys Compd. **299**, 205 (2000).
27. I. I. Tashlykova-Bushkevich and V. G. Shepelevich, Fiz. Khim. Obrab. Mater., No. 4, 99 (2000).
28. I. I. Tashlykova-Bushkevich, in *Proceedings of the 3rd All-Russian Scientific and Technical Conference on Rapidly-Quenched Materials and Coatings*, Ed. by A. P. Petrov, V. A. Vasil'ev, and A. A. Lozovan (Moscow State Aviation Technological University (MATI)–Russian State Technological University (RGTU), Moscow, 2004), p. 23.

29. I. I. Tashlykova-Bushkevich, V. S. Kulikauskas, V. Vesh, et al., Fiz. Khim. Obrab. Mater., No. 3, 75 (2004).
30. I. I. Tashlykova-Bushkevich, E. S. Gut'ko, and V. G. Shepelevich, Poverkhnost, No. 4, 100 (2006).
31. T. S. Srivatson, T. S. Sudarshan, and E. J. Lavernia, Prog. Mater. Sci. **39**, 317 (1995).
32. F. Pleiter and C. Hohenemser, Phys. Rev. B: Condens. Matter **25** (1), 106 (1982).
33. M. de Haas and J. Th. M. de Hosson, Scr. Mater. **44**, 281 (2001).
34. A. Brokman, Acta Metall. **35** (2), 307 (1987).
35. A. R. Knudson, Nucl. Instrum. Methods **168**, 163 (1980).
36. A. A. Klyuchnikov, N. N. Pucherov, T. D. Chesnokova, and V. N. Shcherbin, *Methods of Charged-Particle Beam Analysis* (Naukova Dumka, Kiev, 1987) [in Russian].
37. V. Shepelevich and I. Tashlykova-Bushkevich, Mater. Sci. Forum **248–249**, 385 (1997).
38. V. I. Fadeeva, A. V. Leonov, G. K. Ryasnyi, and S. I. Reiman, Metally, No. 2, 87 (1993).
39. A. Il'inskii, S. Slyusarenko, O. Slukhovskii, et al., Mater. Sci. Eng., A **325** (1–2), 98 (2002).
40. A. G. Khachaturyan, *Theory of Structural Transformations in Solids* (Nauka, Moscow, 1974; Wiley, New York, 1983).
41. A. Guinier, *Heterogeneities in Solid Solutions* (Academic, New York, 1959; Inostrannaya Literatura, Moscow, 1962).
42. R. I. Kuznetsova, S. Z. Fedorenko, G. M. Tsoi, and N. N. Zhukov, Fiz. Met. Metalloved. **42** (1), 75 (1976).
43. V. I. Fadeeva, A. A. Leonov, G. K. Ryasnyi, and A. A. Sorokin, Neorg. Mater. **26** (8), 1662 (1990).
44. H. El. Sayed and I. Kovăcs, Phys. Status Solidi A **24** (1), 123 (1974).
45. I. Kovăcs, Cryst. Res. Technol. **19** (10), 1331 (1984).
46. A. Gaber, N. Afify, and M. S. Mostafa, J. Phys. D: Appl. Phys. **23**, 1119 (1990).
47. D. H. Kim and B. Cantor, Philos. Mag. A **69** (1), 45 (1994).
48. I. I. Tashlykova-Bushkevich and M. Kolasik, in *Proceedings of the IV International Conference on New Electrical and Electronic Technologies and Their Industrial Implementation (NEET'2005)*, Ed. by P. Węgierek and T. Kołtunowicz (Lublin University of Technology, Zakopane, Poland, 2005), p. 175.